ACS APPLIED MATERIALS & INTERFACES

Research Article

www.acsami.org

In Situ DNA-Templated Synthesis of Silver Nanoclusters for Ultrasensitive and Label-Free Electrochemical Detection of MicroRNA

Cuiyun Yang, Kai Shi, Baoting Dou, Yun Xiang,* Yaqin Chai, and Ruo Yuan

Key Laboratory of Luminescent and Real-Time Analytical Chemistry, Ministry of Education, School of Chemistry and Chemical Engineering, Southwest University, Chongqing 400715, P.R. China

Supporting Information

ABSTRACT: On the basis of the use of silver nanoclusters (AgNCs) in situ synthesized by cytosine (C)-rich loop DNA templates as signal amplification labels, the development of a label-free and highly sensitive method for electrochemical detection of microRNA (miRNA-199a) is described. The target miRNA-199a hybridizes with the partial dsDNA probes to initiate the target-assisted polymerization nicking reaction (TAPNR) amplification to produce massive intermediate sequences, which can be captured on the sensing electrode by the self-assembled DNA secondary probes. These surface-captured intermediate sequences further trigger the hybridization chain reaction (HCR) amplification to form dsDNA polymers with numerous C-rich loop DNA templates on the electrode surface. DNA-templated synthesis of AgNCs can be realized by subsequent incubation of the dsDNA polymer-modified electrode with $AgNO_3$ and sodium borohydride. With this integrated TAPNR and HCR dual amplification strategy, the amount of in situ synthesized AgNCs is dramatically enhanced, leading to substantially amplified current response for highly sensitive detection of miRNA-199a down to 0.64 fM. In addition, the developed method also shows high selectivity toward the target miRNA-199a. Featured with high sensitivity and label-free capability, the proposed sensing scheme can thus offer new opportunities for achieving sensitive, selective, and simple detection of different types of microRNA targets.

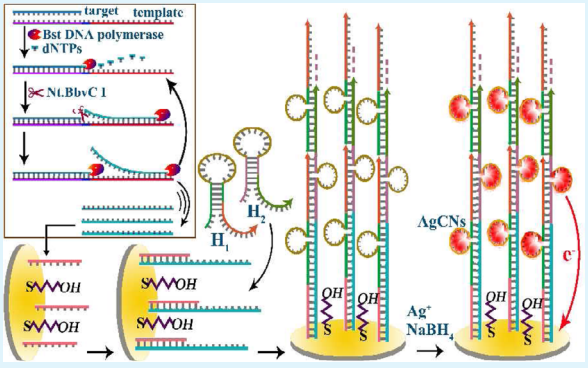

KEYWORDS: *electrochemical, silver nanoclusters, label-free, signal amplification, MicroRNA, serum*

INTRODUCTION

MicroRNAs (miRNAs), typically about 19−25 nucleotides in length produced by digesting single-stranded hairpin structure RNA precursors (about70−90 bases) in the Dicer enzyme processing, are a class of single-stranded, endogenous, non-protein-coding RNAs.[1,2] MiRNAs exhibit a variety of important regulatory roles in the living process by specifically binding to the target messenger RNAs (mRNAs),[3] thereby inhibiting gene expression after transcription, including cell proliferation, differentiation, apoptosis, and metabolism.[4] The regulatory ability of the cellular miRNAs can alter the majority of human mRNA expressions and affect the downstream production of many gene products and eventually the proteins. It has been shown that the aberrant (increased or decreased) expression of miRNA is associated with several diseases, such as cancer,[5] hepatitis,[6,7] malignancies,[8] and neurodegeneration.[9] The expression profiles of miRNAs can thus serve as desirable biomarker candidates for prognosis, diagnosis and even treatment of cancer and other diseases. Therefore, the development of highly sensitive, selective and simple methods for the detection of miRNA is urgently demanded.

Early traditional miRNA detection methods include microarrays,[10] real-time polymerase chain reaction (RT-PCR),[11] Northern blot,[12] in situ hybridization[13] and bioluminescence.[10] The detection approaches of Northern blot and in situ hybridization have low sensitivity and generally require cumbersome steps, limiting their routine applications for miRNA analysis.[14] The RT-PCR assay methods are prone to external contamination due to the extra primer extension amplification techniques, while the microarray approaches require expensive instruments and intricate operations to prevent excitation light or environment effects from quenching fluorescence.[15] The bioluminescence-based miRNA assays, however, need expensive reagents and instruments and the enrichment of the target miRNA as well. These limitations of the traditional miRNA detection methods therefore intrigue the development of new alternatives for miRNA monitoring. In recent years, a number of approaches based on fluorescence,[16−18] electrochemiluminescence (ECL)[19] and electrochemistry[20−22] for miRNA detection have been reported. Among these detection schemes, the electrochemistry-based approaches are particularly suitable for achieving convenient, sensitive and selective detection of miRNA because of the intrinsic advantages

Received: October 8, 2014
Accepted: December 23, 2014
Published: December 23, 2014

DOI: 10.1021/am506933r
ACS Appl. Mater. Interfaces 2015, 7, 1188−1193

Scheme 1. Schematic Illustration of Ultrasensitive and Label-Free Electrochemical Detection of miRNA-199a Based on In Situ Generated AgNCs by Coupling TAPNR with HCR Amplifications

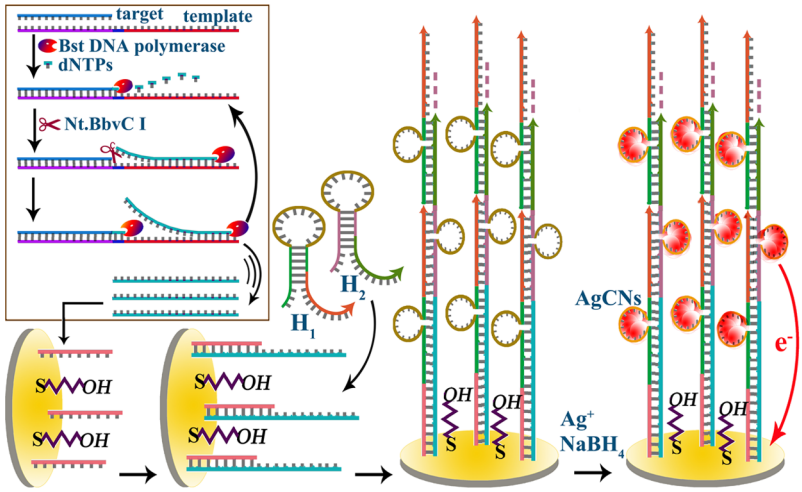

of the electrochemical techniques in terms of simplicity, easy miniaturization, low cost, and high sensitivity.

To achieve sensitive detection of miRNA, electrochemical labels are commonly used to amplify the signal output, and a variety of nanomaterials are increasingly employed as effective signal enhancers, because of their unique electronic and catalytic properties, as well as their high specific surface area and the high loading capacity for the receptor molecules.[23−25] However, extensive conjugation of the nanomaterial labels to the probe molecules is commonly required in most electrochemical assays, which potentially increases the complexity and cost of the methods. The development of label-free, nanomaterial-based amplification strategies would therefore facilitate the monitoring of miRNA.

Herein, we report on a new label-free strategy for highly sensitive detection of miRNA (miRNA-199a) based on in situ, DNA template-synthesized silver cluster (AgNC) signal amplification labels. AgNCs are ultrasmall particles containing 2−30 of Ag atoms.[26] These AgNCs exhibit dramatically different optical, electronic, and chemical properties when compared to nanoparticles or bulk materials due to their extremely small sizes.[27,28] Since the first report on DNA-templated synthesis of AgNCs by Dickson's group in 2004,[29] AgNCs have been widely used as fluorescent tags in live cell staining[30] and the detection of different types of molecules such as metal ions,[31] small molecules,[32] DNA[33] and proteins.[34] Although increasingly used as fluorescent tags, the employment of AgNCs as electrochemical labels has been rarely explored.[35] Similar to the redox property of Ag nanoparticles, AgNCs can be potentially used as electrochemical tags for amplified detections.[36] Besides, in our miRNA detection approach, two amplification strategies, target-assisted polymerization nicking reaction (TAPNR) and hybridization chain reaction (HCR),[37] are incorporated into the assay method to increase the amount of the in situ-synthesized AgNCs to achieve subfemtomolar detection of miRNA-199a.

EXPERIMENTAL SECTION

Chemicals and Materials. Tris-HCl, tris(2-carboxyethyl) phosphine hydrochloride (TCEP), and 6-mercapto-1-hexanol (MCH) were purchased from Sigma-Aldrich (St. Louis, MO). The nicking enzyme Nt.BbvCI (an endonuclease that recognizes the specific nucleotide sequence of 5′-CC↓TCAGC-3′ in a dsDNA and cuts the nucleotide sequence in the arrow), Bst-DNA polymerase (Large Fragment) and NEB buffer (10 ×) (50 mM NaCl, 10 mM Tris-HCl, 10 mM $MgCl_2$, 1 mM dithiothreitol, pH 7.9) were purchased from New England Biolabs Inc. (Beijing, China). Ethylenediaminetetraacetic acid (EDTA), sodium citrate and sodium borohydride ($NaBH_4$) were obtained from Kelong Chemical Inc. (Chengdu, China). Silver nitrate ($AgNO_3$) was purchased from Aladdin Reagents (Shanghai, China).

The HPLC-purified miRNAs, all synthetic DNAs with sequences listed below and the deoxyribonucleoside 5′-triphosphate (dNTPs) mixture were all provided by Invitrogen Biotechnology Co. Ltd. (Shanghai, China). Target miRNA-199a: 5′-ACA GUA GUC UGC ACA UUG GUU A-3′; MiRNA-21:5′-UAG CUU AUC AGA CUG AUG UUG A-3′; MiRNA-141:5′- UAA CAC UGU CUG GUA AAG AUG G-3′; one-base mismatched miRNA-199a: 5′-ACA GUC GUC UGC ACA UUG GUU A-3′; Three-base mismatched miRNA-199a: 5′-ACA GUC GUC UGA ACC UUG GUU A-3′; amplification template probe (TP): 5′-TTA CAT AAG GCT GAT CAG CTG AGG TAA CCA ATG TGC AGA CTA CTG T-3′; thiolated capture probe (SH−CP): 5′-SH-TTA CAT AAG-3′; hairpin probe H_1: 5′-GCT GAT CAG CCC CCC CCC CCC CTG ATC TGC ATC TAG AT-3′; hairpin probe H_2: 5′-TCA GCT GAT CAG CAT CTC CCC CCC CCC CCA GAT GCA GA-3′; hairpin probe H_1 without the C-rich region: 5′- GCT GAT CAG TTA GAT TAG ATT CTG ATC TGC ATC TAG AT-3′; hairpin probe H_2 without the C-rich region: 5′- TCA GCT GAT CAG CAT CTT TAG ATT AGA TTA GAT GCA GA-3′. All reagents were analytical grade and solutions were prepared using ultrapure water (specific resistance of 18 MΩ-cm).

Target-Assisted Polymerization Nicking Reaction (TAPNR). The TAPNR was carried out by incubating the mixture of TP (1.0 μM), Bst-DNA polymerase (0.4 U), Nt.BbvCI nicking enzyme (0.2 U), dNTPs (250 μM) and a series of various concentration of the target miRNA-199a in 1 × NEB buffer at 37 °C for 60 min to produce massive intermediate sequences. After that, the mixtures were heated to 90 °C and kept for 10 min to deactivate the Bst-DNA polymerase and Nt.BbvCI enzyme, followed by cooling down to room temperature.

Label-Free and Amplified Electrochemical Detection of miRNA-199a. First of all, the gold electrodes (AuEs, 3 mm in diameter) were soaked in fresh piranha solution (mixture of 98% H_2SO_4 and 30% H_2O_2 at a volume ratio of 3:1) for at least 30 min, followed by polishing with 0.3 and 0.05 μm alumina slurries for 5 min separately after rinsing thoroughly with ultrapure water. After that, the electrodes were sonicated sequentially for 5 min in ultrapure water, ethanol and ultrapure water to remove the residual alumina powder. Then, the electrodes were further electrochemically cleaned in 0.5 M H_2SO_4 with potential scanning from −0.3 and 1.55 V until a remarkable voltammetric peak was obtained, followed by rinsing with ultrapure water and drying with nitrogen. Next, a droplet of 10 μL SH−CP (0.5

DOI: 10.1021/am506933r
ACS Appl. Mater. Interfaces 2015, 7, 1188−1193

μM) in the immobilization buffer (10 mM Tris-HCl, 1 mM EDTA, 10 mM TCEP, 0.1 M NaCl, pH 7.4) was dropped on the pretreated electrodes and incubated overnight at room temperature. After being rinsed with deionized water, the resulting SH−CP-assembled electrode was blocked with 1 mM MCH (10 μL) for 2 h to obtain the MCH/SH−CP/AuE. After rinsed and dried, the MCH/SH−CP/AuE modified electrode was then incubated with the mixture of the reaction product of TAPNR for 1 h at room temperature to capture the intermediate sequences on the gold sensing electrodes by their complementary sequences (SH−CP) through DNA hybridizations. Followed by washing with HB buffer (10 mM Tris-HCl, 500 mM NaCl and 1 mM $MgCl_2$, pH 7.4), the electrodes were exposed to the mixture of H_1 (0.5 μM) and H_2 (0.5 μM) in HB at room temperature for 2 h. Then, the electrodes were rinsed with HB and dried, and 10 μL of $AgNO_3$ solution (100 μM) in citrate buffer (20 mM sodium citrate, pH 7.0) was dropped on the electrode surface for 15 min in dark. Subsequently, 2 μL of fresh $NaBH_4$ solution (500 μM) in citrate buffer was carefully added to the electrode surface covered by $AgNO_3$ solution at room temperature for 2 h in dark to reduce $AgNO_3$ to AgNCs.[38] Finally, the electrodes were washed with phosphate buffer (PB, 0.15 M, pH 5.5) and electrochemical measurements were performed.

Electrochemical Measurements. Cyclic voltammetry (CV) and differential pulse voltammetry (DPV) were performed on a CHI 621D electrochemistry workstation (CH Instruments Inc., Shanghai, China). A conventional three-electrode system with a Ag/AgCl (3 M KCl) reference electrode, a platinum wire counter electrode, and the modified AuE was used for the measurements. DPV measurements were carried out in PB by scanning the potential from 0.0 to 0.4 V with the pulse amplitude of 50 mV, pulse width of 25 ms and sampling width of 16.7 ms.

RESULTS AND DISCUSSION

Scheme 1 illustrates our approach for highly sensitive and label-free electrochemical detection of miRNA-199a based on the in situ-synthesized AgNCs. To achieve significant signal enhancement, two amplification means, TAPNR and HCR, are integrated into the assay protocol. As depicted in Scheme 1, in the TAPNR process, the target miRNA-199a first hybridizes with the amplification template probe (TP). TP contains three functional regions: a miRNA-binding domain that is complementary to the target miRNA-199a (the pink region), a complementary domain of the recognition sequences for the nicking enzymes Nt.BbvCI (the short blue region in the middle of TP), and an amplification domain (the red region) that acts as the template to produce massive intermediate sequences (the cyan sequence) with the aid of the Bst-DNA polymerase and Nt.BbvCI nicking enzyme. Upon the formation of the partial duplex by the hybridization between the miRNA-199a and TP, the Bst-DNA polymerase (with the presence of dNTPs) catalyzes the extension of miRNA-199a starting from the 3′ terminus to form fully complementary duplex with specific recognition sequence (5′-CC$^{\downarrow}$TCAGC-3′) and site (in the arrow) for the Nt.BbvCI nicking enzyme, which cleaves the fully complementary duplex and releases the intermediate sequence. The release of the intermediate sequence can result in another round of polymerase extension of the miRNA-199a and the generation of duplicated intermediate sequences. By following this TAPNR mechanism, the generation of the intermediate sequences is amplified exponentially and numerous intermediate sequences can thus be produced. After the completion of the TAPNR, these intermediate sequences are captured by the SH−CPs self-assembled on the AuE and further trigger the HCR formation of the dsDNA ploymers on the AuE with the presence of the cytosine (C)-rich loop hairpin probes (H_1 and H_2),[39] which can facilitate the formation of stable AgNCs.[40] After HCR, DNA polymers with multiple C-rich loop hairpins are assembled on the electrode surface and numerous AgNCs can thus be in situ generated upon incubation of the electrode with $AgNO_3$ and $NaBH_4$. These in situ-generated AgNCs are expected to exhibit substantially amplified current response under DPV scan for indirect detection of trace amounts of miRNA-199a.

CV, an effective tool for the investigation of self-assembled monolayers on the electrode surface, was employed to characterize the fabrication process of the electrochemical biosensor at different stages with the sensitive redox couple of $[Fe(CN)_6]^{3-/4-}$ in KCl solution (0.1 M). As shown in Figure 1, a

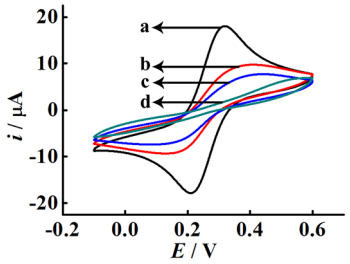

Figure 1. Typical cyclic voltammograms of different modified electrode: (a) bare AuE, (b) SH−CP/AuE, (c) intermediate sequence/SH−CP/AuE, and (d) HCR/intermediate sequence/SH−CP/AuE. CV measurements were performed in 0.1 M KCl solution containing 1 mM $[Fe(CN)_6]^{3-/4-}$ by scanning the potential from −0.1 to 0.6 V at a scan rate of 50 mV S^{1-}.

couple of reversible, well-defined redox peaks of $[Fe(CN)_6]^{3-/4-}$ (curve a) with maximum current intensity is observed on the pretreated bare AuE because of the strong electron transfer ability of $[Fe(CN)_6]^{3-/4-}$ to the bare AuE. After the formation of the self-assembled monolayer of the SH−CP and MCH on the pretreated AuE, the current responses of $[Fe(CN)_6]^{3-/4-}$ exhibit dramatic decreases (curve b vs a), because of the electrostatic repulsion of $[Fe(CN)_6]^{3-/4-}$ from the electrode surface by the negative charges on the DNA backbones. As expected, the hybridizations between the intermediate sequences (generated by the TAPNR process) and the self-assembled SH−CPs lead to further deceases in the current responses (curve c) due to the introduction of more negative charges to the electrode surface. Subsequent HCR triggered by the surface-hybridized intermediate sequences causes significant suppression of current responses and dramatic peak separation (curve d) because of the formation of the dsDNA polymers on the electrode surface. These results suggest the successful fabrication of the self-assembled monolayer and surface-initiated HCR on the sensing electrode.

To verify the signal amplification capability of our new protocol, the signal outputs with/without the TAPNR and HCR amplifications were first compared in the absence/presence of the miRNA-199a (10 pM) target sequences (see Figure 2). In the absence of miRNA-199a, the TAPNR amplification process is inhibited, subsequent generation of the intermediate sequences is suppressed, and a small background current response at ~0.24 V (curve a) is observed because of the direct adsorption of Ag^+ on the self-assembled SH−CP by electrostatic interaction between the negatively charged DNA backbones and the positively charged Ag^+ and reduction by $NaBH_4$.[41] In the presence of miRNA-199a (10 pM), the TAPNR process proceeds to generate massive intermediate sequences, which hybridize with the SH−CPs on the AuE. The capture of the intermediate sequences (without subsequent HCR) leads to apparent increase in the current response (curve b) due to the adsorption of more

DOI: 10.1021/am506933r
ACS Appl. Mater. Interfaces 2015, 7, 1188−1193

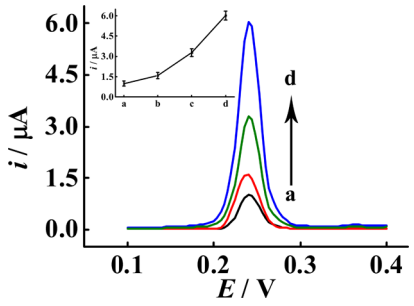

Figure 2. Typical DPV responses of the sensing electrodes for (a) the absence and (b) the presence of miRNA-199a (10 pM) with TAPNR amplification, (c) the presence of miRNA-199a (10 pM) with both TAPNR and HCR by using H_1 and H_2 without and (d) with the C-rich loop regions. The immobilization concentration of SH−CP: 0.5 μM; The TAPNR time: 50 min; The concentration of $AgNO_3$: 200 μM. DPV measurements were performed in 0.15 M PB (pH 5.5) with the pulse amplitude of 50 mV, pulse width of 25 ms and sampling width of 16.7 ms. Error bars, SD, n = 3.

Ag^+ on the DNA strands. Subsequent HCR assembly of H1 and H2 without the C-rich loop regions on the electrode surface results in further increase in current response (curve c) because of the enhanced adsorption of Ag^+ instead of the formation of the AgNCs on the self-assembled DNA polymers. Moreover, when H1 and H2 with the C-rich loop regions are self-assembled on the electrode surface through the intermediate sequence-triggered HCR, significant amplification of the current response is observed (curve d), which is due to the electro-oxidation of the DNA-templated, in situ synthesized AgNCs. The experimental comparisons here clearly indicate the significant signal amplification capability of the proposed method for miRNA-199a detection via the combination of the TAPNR and HCR dual signal amplification strategy.

To achieve optimal performance for amplified electrochemical detection of miRNA-199a by using our approach, the effect of different assay parameters, including the immobilization concentration of SH−CP, TAPNR time, and the concentration of $AgNO_3$, on the signal output were investigated. On the basis of our previous report on surface initiated HCR, the HCR time was fixed at 2 h in all experiments.[39] We first optimized the immobilization concentration of SH−CP at 0.2, 0.5, and 1.0 μM, respectively, for the detection of miRNA-199a (10 pM). As shown in Figure 3A, the immobilization concentration of SH−CP at 0.5 μM exhibits the best signal-to-noise ratio (i/i_0, i and i_0 correspond to the DPV peak currents with the presence and absence of the target miRNA-199a, respectively) for miRNA-199a. Although the low density of SH−CP (0.2 μM) results in a low background current due to decreased adsorption of Ag^+, the DPV signal current response with the presence of the target miRNA-199a is also low because of the reduced capture of the intermediate sequences for subsequent HCR. This leads to a lower signal-to-noise ratio. High density of SH−CP (1.0 μM) results in a slightly decreased current response for the presence of the target miRNA-199a. Such decrease is possibly due to the partial inhibition of HCR by the steric hindrance of the increased amount of the intermediate sequences captured by the high density of SH−CP. On the other hand, high density of SH−CP also leads to the adsorption of more Ag^+ and relatively high background, and the lowest signal-to-noise is obtained. According to the results, the medium density (0.5 μM) of SH−CP is selected as the optimal immobilization concentration for all subsequent experiments. Figure 3B depicts the effect of the TAPNR time on the DPV response in the presence of the target miRNA-199a (10 pM). As anticipated, the DPV peak current increases rapidly along with the extension of the TAPNR duration and reaches a plateau at 60 min, which is due to the fact that with longer TAPNR time, more intermediate sequences can be generated and captured by SH−CP to trigger the HCR amplification. However, the amount of intermediate sequences captured on the electrode is close to saturation with the TAPNR for 60 min, leading to the plateau in Figure 3B. Based on the results, 60 min is selected as the optimal TAPNR duration. Considering the important role of $AgNO_3$ in the synthesis of the AgNCs, the effect of the concentration of $AgNO_3$ on the signal-to-noise ratio was also investigated. From Figure 3C, we can see that the vlaue of i/i_0 increases gradually with increasing incubation concentration of $AgNO_3$ from 20 μM to 100 μM and decreases thereafter (from 100 to 500 μM). Such a decrease is assumably due to the reason that the synthesis of AgNCs tends to saturate at the concentration of $AgNO_3$ higher than 100 μM, whereas a further increase in the concentration of $AgNO_3$ is prone to cause an increase in the background current, resulting in decreased i/i_0 value. The concentration of $AgNO_3$ is therefore fixed at 100 μM for subsequent experiments.

The DPV response of the sensor for different concentrations of the target miRNA-199a was measured to serve as the basic values for miRNA-199a determination. As shown in Figure 4A, the DPV response increases accordingly with increasing concentration of miRNA-199a from 1.0 fM to 0.1 nM under optimized conditions. Figure 4B displays the calibration curve for quantitative analysis of the target miRNA-199a, in which the DPV peak current response shows a strong linear dependence upon the logarithm of the concentration of the target miRNA-199a. The linear regression equation is determined to be i (μA) = 14.9753 + 0.9428 log c (i is the peak current and c is the

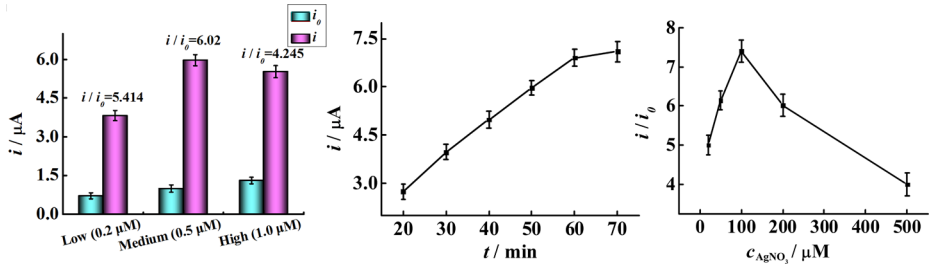

Figure 3. Optimization of (A) immobilization concentration of SH−CP (with the TAPNR time for 50 min and the concentration of $AgNO_3$ at 200 μM), (B) TAPNR time (with immobilization concentration of SH−CP at 0.5 μM and the concentration of $AgNO_3$ at 200 μM), and (C) the concentration of $AgNO_3$ (with the immobilization concentration of SH−CP at 0.5 μM and the TAPNR time for 60 min) for amplified detection of miRNA-199a (10 pM) by using the proposed sensing method. Error bars: SD, n = 3. Other conditions, as in Figure 2.

DOI: 10.1021/am506933r
ACS Appl. Mater. Interfaces 2015, 7, 1188−1193

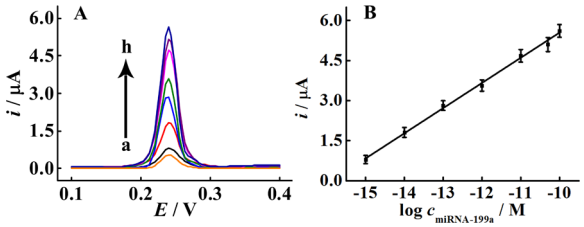

Figure 4. (A) Typical DPV responses of the proposed sensor for different concentrations of the target miRNA-199a: (a) 0 fM, (b) 1.0 fM, (c) 10 fM, (d) 0.1 pM, (e) 1.0 pM, (f) 10 pM, (g) 50 pM, and (h) 0.1 nM. (B) The resulting calibration plot of i vs log c. Error bars, SD, $n = 3$. Other conditions, as in Figure 2

concentration of the target miRNA-199a) with a correlation coefficient (R^2) of 0.9972 and the detection limit is estimated to be 0.64 fM (three times the standard deviation above the blank, $n = 11$). In addition, the relative standard deviation ($n = 6$) of the target miRNA-199a at the 10 pM level was 6.7% with different electrodes, indicating good reproducibility of the proposed sensing method.

The selectivity of the proposed method was evaluated by using four control microRNA sequences, including the miRNA-21, miRNA-141, and one- and three-base mismatched miRNA-199a sequences. As exhibited in Figure 5 (bar b to d), the DPV peak

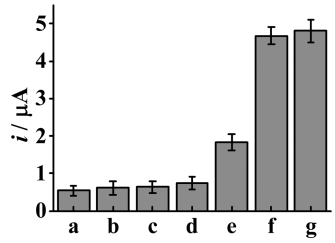

Figure 5. Selectivity investigation of the proposed method for (a) blank solution (in the absence of the target miRNA-199a), (b) miRNA-21 (0.5 nM), (c) miRNA-141 (0.5 nM), (d) three-base mismatched miRNA-199a (0.5 nM), (e) one-base mismatched miRNA-199a (0.5 nM), (f) miRNA-199a (10 pM), and (g) mixture of miRNA-199a (10 pM), miR-21 (0.5 nM), miR-141 (0.5 nM), and three-base mismatched miRNA-199a (0.5 nM). Error bars, SD, $n = 3$. Other conditions, as in Figure 2

currents for the presence of the control sequences (miRNA-21, miRNA-141 and three-base mismatched miRNA-199a all at 0.5 nM) show insignificant changes compared to that of the blank test (bar a, background current with the absence of the target miRNA-199a). Despite the apparent increase in the peak current for the one-base mismatched miRNA-199a (bar e), the presence of a much lower (50-fold) concentration of the target miRNA-199a (10 pM) yields a significantly higher DPV peak current, and the mixture of the target miRNA-199a (10 pM) with miRNA-21, miRNA-141 and three-base mismatched miRNA-199a (each at 0.5 nM) has negligibly influence on the current intensity (bar g vs f). These comparisons indicate the high selectivity of the method, in which only the perfectly complementary miRNA can trigger the TAPNR and HCR amplifications to generate significantly enhanced current response. That is to say, the developed detection method is highly selectively toward miRNA-199a against other control sequences.

The feasibility of the sensing strategy for the detection of miRNA-199a in real samples were evaluated by performing recovery tests of miRNA-199a in human serum samples (obtained from healthy volunteer) using the standard addition method. Different concentrations of miRNA-199a at 10 fM, 1.0 pM, 50 pM were separately spiked into the serum samples diluted 10 times with 1 × NEB buffer and the measured results are shown in Table 1. From this table, we can see that the

Table 1. Detection of miRNA-199a in Human Serum Samples Using the Proposed Method ($n = 6$)

sample	added	found	rate of recovery (%)	RSD (%)
1	10 fM	9.8 fM	96.5−102.6	4.8
2	1.0 pM	1.04 pM	98.9−103.8	3.8
3	50 pM	49.7 pM	97.2−101.9	4.5

recoveries for the added miRNA-199a are in the range from 96.5 to 103.8%, and the RSD is below 4.8%, indicating that the proposed sensing platform can be applied to monitor miRNA-199a in complex biological samples.

CONCLUSIONS

In summary, we have demonstrated a label-free and highly sensitive method for electrochemical detection of miRNA-199a by using AgNC labels. The AgNC signal amplification labels can be synthesized in situ on the sensing electrode to avoid any signal probe conjugation steps to achieve label-free detection of miRNA-199a. Besides, the TAPNR and HCR amplification approaches are integrated into the assay protocol to assemble multiple C-rich loop DNA templates on the electrode surface to increase the synthesis of AgNCs, which leads to significantly enhanced current response for highly sensitive detection of miRNA-199a at 0.64 fM. Moreover, the developed method is also selective toward the target miRNA-199a against other control microRNA sequences and can be used to detect miRNA in human serum samples. With the advantages in terms of label-free and high sensitivity, we expect the developed microRNA detection method to be expanded for the monitoring of more general nucleic acid sequences in addition to microRNA targets at ultralow levels.

ASSOCIATED CONTENT

Supporting Information

Materials including the TEM image of the AgNCs and the measurement of the surface probe density. This material is available free of charge via the Internet at http://pubs.acs.org/.

AUTHOR INFORMATION

Corresponding Author

*E-mail: yunatswu@swu.edu.cn. Tel./Fax: +86-23-68252277.

Notes

The authors declare no competing financial interest.

ACKNOWLEDGMENTS

This work was supported by NSFC (21275004 and 21275119), the New Century Excellent Talent Program of MOE (NCET-12-0932) and Fundamental Research Funds for the Central Universities (XDJK2014A012).

REFERENCES

(1) Bernstein, E.; Caudy, A. A.; Hammond, S. M.; Hannon, G. J. Role for a Bidentate Ribonuclease in the Initiation Step of RNA Interference. *Nature* **2001**, *409*, 363−366.

(2) MacRae, I. J.; Zhou, K.; Li, F.; Repic, A.; Brooks, A. N.; Cande, W. Z.; Adams, P. D.; Doudna, J. A. Structural Basis for Double-Stranded RNA Processing by Dicer. *Science* **2006**, *311*, 195−198.

DOI: 10.1021/am506933r
ACS Appl. Mater. Interfaces 2015, 7, 1188−1193

(3) Martinez, N. J.; Gregory, R. I. MicroRNA Gene Regulatory Pathways in the Establishment and Maintenance of ESC Identity. *Cell Stem Cell* **2010**, *7*, 31−35.
(4) Zhou, Y. L.; Zhang, Z. Y.; Xu, Z. N.; Yin, H. S.; Ai, S. Y. MicroRNA-21 Detection Based on Molecular Switching by Amperometry. *New J. Chem.* **2012**, *36*, 1985−1991.
(5) Hizir, M. S.; Balcioglu, M.; Rana, M.; Robertson, N. M.; Yigit, M. V. Simultaneous Detection of Circulating OncomiRs from Body Fluids for Prostate Cancer Staging Using Nanographene Oxide. *ACS Appl. Mater. Interfaces* **2014**, *6*, 14772−14778.
(6) Jopling, C. L.; Yi, M. K.; Lancaster, A. M.; Lemon, S. M.; Sarnow, P. Modulation of Hepatitis C Virus RNA Abundance by a Liver-Specific MicroRNA. *Science* **2005**, *309*, 1577−1581.
(7) Huang, J. F.; Wang, Y.; Guo, Y. G.; Sun, S. H. Down-Regulated MicroRNA-152 Induces Aberrant DNA Methylation in Hepatitis B Virus-Related Hepatocellular Carcinoma by Targeting DNA Methyltransferase. *Hepatology* **2010**, *52*, 60−70.
(8) Huang, R. C.; Chiu, W. J.; Li, Y. J.; Huang, C. C. Detection of MicroRNA in Tumor Cells Using Exonuclease III and Graphene Oxide-Regulated Signal Amplification. *ACS Appl. Mater. Interfaces* **2014**, DOI: 10.1021/am500534g.
(9) Hébert, S. S.; De Strooper, B. Molecular Biology. MiRNAs in Neurodegeneration. *Science* **2007**, *317*, 1179−1180.
(10) Cissell, K. A.; Rahimi, Y.; Shrestha, S.; Hunt, E. A.; Deo, S. K. Bioluminescence-Based Detection of MicroRNA, MiR21 in Breast Cancer Cells. *Anal. Chem.* **2008**, *80*, 2319−2325.
(11) Chen, C. F.; Ridzon, D. A.; Broomer, A. J.; Zhou, Z. H.; Lee, D. H.; Nguyen, J. T.; Barbisin, M.; Xu, N. L.; Mahuvakar, V. R.; Andersen, M. R.; Lao, K. Q.; Livak, K. J.; Guegler, K. J. Real-Time Quantification of MicroRNAs by Stem-Loop RT-PCR. *Nucleic Acids Res.* **2005**, *33*, 179−187.
(12) Válóczi, A.; Hornyik, C.; Varga, N.; Burgyán, J.; Kauppinen, S.; Havelda, Z. Sensitive and Specific Detection of MicroRNAs by Northern Blot Analysis Using LNA-Modified Oligonucleotide Probes. *Nucleic Acids Res.* **2004**, *32*, 175−181.
(13) Deo, M.; Yu, J. Y.; Chung, K. H.; Tippens, M.; Turner, D. L. Detection of Mammalian MicroRNA Expression by in Situ Hybridization with RNA Oligonucleotides. *Dev. Dyn.* **2006**, *235*, 2538−2548.
(14) Catuogno, S.; Esposito, C. L.; Quintavalle, C.; Cerchia, L.; Condorelli, G.; de Franciscis, V. Recent Advance in Biosensors for MicroRNAs Detection in Cancer. *Cancers* **2011**, *3*, 1877−1898.
(15) Castoldi, M.; Schmidt, S.; Benes, S.; Hentze, M. W.; Muckenthaler, M. U. MiChip: an Array-Based Method for MicroRNA Expression Profiling Using Locked Nucleic Acid Capture Probes. *Nat. Protoc.* **2008**, *3*, 321−329.
(16) Su, S.; Fan, J. W.; Xue, B.; Yuwen, L. H.; Liu, X. F.; Pan, D.; Fan, C. H.; Wang, L. H. DNA-Conjugated Quantum Dot Nanoprobe for High-Sensitivity Fluorescent Detection of DNA and Micro-RNA. *ACS Appl. Mater. Interfaces* **2014**, *6*, 1152−1157.
(17) Yuan, Z.; Zhou, Y. Y.; Gao, S. X.; Cheng, Y. Q.; Li, Z. P. Homogeneous and Sensitive Detection of microRNA with Ligase Chain Reaction and Lambda Exonuclease-Assisted Cationic Conjugated Polymer Biosensing. *ACS Appl. Mater. Interfaces* **2014**, *6*, 6181−6185.
(18) Yang, L.; Liu, C. H.; Ren, W.; Li, Z. P. Graphene Surface-Anchored Fluorescence Sensor for Sensitive Detection of MicroRNA Coupled with Enzyme-Free Signal Amplification of Hybridization Chain Reaction. *ACS Appl. Mater. Interfaces* **2012**, *4*, 6450−6453.
(19) Cheng, Y.; Lei, J. P.; Chen, Y. L.; Ju, H. X. Highly Selective Detection of MicroRNA Based on Distance-Dependent Electrochemiluminescence Resonance Energy Transfer Between CdTe Nanocrystals and Au Nanoclusters. *Biosens. Bioelectron.* **2014**, *51*, 431−436.
(20) Labib, M.; Khan, N.; Ghobadloo, S. M.; Cheng, J.; Pezacki, J. P.; Berezovski, M. V. Three-Mode Electrochemical Sensing of Ultralow MicroRNA Levels. *J. Am. Chem. Soc.* **2013**, *135*, 3027−3038.
(21) Labib, M.; Ghobadloo, S. M.; Khan, N.; Kolpashchikov, D. M.; Berezovski, M. V. Four-Way Junction Formation Promoting Ultrasensitive Electrochemical Detection. *Anal. Chem.* **2013**, *85*, 9422−9427.
(22) Lusi, E. A.; Passamano, M.; Guarascio, P.; Scarpa, A.; Schiavo, L. Innovative Electrochemical Approach for an Early Detection of microRNAs. *Anal. Chem.* **2009**, *81*, 2819−2822.
(23) Rosi, N. L.; Mirkin, C. A. Nanostructures in Biodiagnostics. *Chem. Rev.* **2005**, *105*, 1547−1562.
(24) Li, Q. F.; Zeng, L. X.; Wang, J. C.; Tang, D. P.; Liu, B. Q.; Chen, G. N.; Wei, M. D. Magnetic Mesoporous Organic-Inorganic $NiCo_2O_4$ Hybrid Nanomaterials for Electrochemical Immunosensors. *ACS Appl. Mater. Interfaces* **2011**, *3*, 1366−1373.
(25) Miao, P.; Han, K.; Sun, H. X.; Yin, J.; Zhao, J.; Wang, B. D.; Tang, Y. G. Melamine Functionalized Silver Nanoparticles as the Probe for Electrochemical Sensing of Clenbuterol. *ACS Appl. Mater. Interfaces* **2014**, *6*, 8667−8672.
(26) Zheng, J.; Nicovich, P. R.; Dickson, R. M. Highly Fluorescent Noble-Metal Quantum Dots. *Annu. Rev. Phys. Chem.* **2007**, *58*, 409−431.
(27) Wilcoxon, J. P.; Abrams, B. L. Synthesis, Structure and Properties of Metal Nanoclusters. *Chem. Soc. Rev.* **2006**, *35*, 1162−1194.
(28) Xu, H. X.; Suslick, K. S. Sonochemical Synthesis of Highly Fluorescent Ag Nanoclusters. *ACS Nano* **2010**, *4*, 3209−3214.
(29) Petty, J. T.; Zheng, J.; Hud, N. V.; Dickson, R. M. DNA-Templated Ag Nanocluster Formation. *J. Am. Chem. Soc.* **2004**, *126*, 5207−5212.
(30) Han, B. Y.; Wang, E. K. DNA-Templated Fluorescent Silver Nanoclusters. *Anal. Bloanal. Chem.* **2012**, *402*, 129−138.
(31) Dong, H. F.; Hao, K. H.; Tian, Y. P.; Jin, S.; Lu, H. T.; Zhou, S. F.; Zhang, X. J. Label-Free and Ultrasensitive MicroRNA Detection Based on Novel Molecular Beacon Binding Readout and Target Recycling Amplification. *Biosens. Bioelectron.* **2014**, *53*, 377−383.
(32) Zhou, Z. X.; Du, Y.; Dong, S. J. DNA-Ag Nanoclusters as Fluorescence Probe for Turn-on Aptamer Sensor of Small Molecules. *Biosens. Bioelectron.* **2011**, *28*, 33−37.
(33) Zhang, L. B.; Zhu, J. B.; Zhou, Z. X.; Guo, S. J.; Li, J.; Dong, S. J.; Wang, E. K. A New Approach to Light up DNA/Ag Nanocluster-Based Beacons for Bioanalysis. *Chem. Sci.* **2013**, *4*, 4004−4010.
(34) Liu, J. J.; Song, X. R.; Wang, Y. W.; Zheng, A. X.; Chen, G. N.; Yang, H. H. Label-Free and Fluorescence Turn-on Aptasensor for Protein Detection via Target-Induced Silver Nanoclusters Formation. *Anal. Chim. Acta* **2012**, *749*, 70−74.
(35) Dong, H. F.; Jin, S.; Ju, H. X.; Hao, K. H.; Xu, L. P.; Lu, H. T.; Zhang, X. J. Trace and Label-Free MicroRNA Detection Using Oligonucleotide Encapsulated Silver Nanoclusters as Probes. *Anal. Chem.* **2012**, *84*, 8670−8674.
(36) Zhang, B.; Liu, B. Q.; Zhou, J.; Tang, J.; Tang, D. P. Additional Molecular Biological Amplification Strategy for Enhanced Sensitivity of Monitoring Low-Abundance Protein with Dual Nanotags. *ACS Appl. Mater. Interfaces* **2013**, *5*, 4479−4485.
(37) Dirks, R. M.; Pierce, N. A. Triggered Amplification by Hybridization Chain Reaction. *Proc. Natl. Acad. Sci. U.S.A.* **2004**, *101*, 1527−15278.
(38) Rao, T. U. B.; Nataraju, B.; Pradeep, T. Ag9 Quantum Cluster through a Solid-State Route. *J. Am. Chem. Soc.* **2010**, *132*, 16304−16307.
(39) Chen, Y.; Xu, J.; Su, J.; Xiang, Y.; Yuan, R.; Chai, Y. Q. In Situ Hybridization Chain Reaction Amplification for Universal and Highly Sensitive Electrochemiluminescent Detection of DNA. *Anal. Chem.* **2012**, *84*, 7750−7755.
(40) Orbach, R.; Guo, W. W.; Wang, F.; Lioubashevski, O.; Willner, I. Self-Assembly of Luminescent Ag Nanocluster-Functionalized Nanowires. *Langmuir* **2013**, *29*, 13066−13071.
(41) Zhang, J.; Ting, B. P.; Jana, N. R.; Gao, Z. Q.; Ying, J. Y. Ultrasensitive Electrochemical DNA Biosensors Based on the Detection of a Highly Characteristic Solid-State Process. *Small* **2009**, *5*, 1414−1417.

DOI: 10.1021/am506933r
ACS Appl. Mater. Interfaces 2015, 7, 1188−1193